

Numerical simulations of sink flow in the Hele-Shaw cell with small surface tension

E. D. KELLY and E. J. HINCH

DAMTP, University of Cambridge, Silver St., Cambridge CB3 9EW, UK

(Received 29 January 1996; in revised form 19 August 1996)

The motion of an initially circular drop of viscous fluid surrounded by inviscid fluid in a Hele-Shaw cell withdrawn from an eccentric point sink is considered. Using a numerical algorithm based on a boundary integral equation, the solution for small, finite surface tension is observed. It is found that the zero-surface-tension formation of a cusp is avoided, and instead a narrow finger of inviscid fluid forms, which then rapidly propagates towards the sink. The scaling of the finger in the sink vicinity is determined.

1 Introduction

1.1 Case of zero surface tension

As detailed in Howison, Lacey & Ockendon (1988), for the Hele-Shaw suction problem with zero surface tension, we have two classes of problems: solutions which do not develop singularities in finite time, and those which do. In the former case we have three sub-classes: (i) solutions removing all the fluid from a finite region. For a given suction mechanism DiBenedetto & Friedman (1984) have shown that there is only one initial shape from which all the fluid may be extracted without singularities forming. In the case of a point sink (the case we shall be concentrating on), a concentric circle of fluid is the only such shape; (ii) solutions leaving residual fluid in an infinite region, for example, the evolution of a finger in the Saffman–Taylor problem (1958); and (iii) solutions removing all the fluid from an infinite region.

On the other hand, singularities such as a cusp on the surface can develop in a finite time (Polubarinova-Kochina, 1945). Starting from an initial limaçon of fluid containing a sink, Howison *et al.* (1985) demonstrate how a three-halves power cusp is formed. In this simple suction case, the analytic solution breaks down at the formation of the cusp, and no continuation beyond the time of formation of the singularity is possible. In fact, the time reversibility of the Hele-Shaw problem with no surface tension leads to the conclusion that a constant-suction mechanism can only cause the fluid domain to shrink to zero in finite time if the fluid domain itself can be produced by the corresponding blowing mechanism starting with no fluid present.

Richardson (1972) solved the problem of injecting into an initially circular domain from an off-centre point. Due to the time-reversibility of the Hele-Shaw equations this analysis could then be used to study the complementary problem of suction, rather than injection, in this geometry up to the point of cusp formation. Richardson has recently (1994)

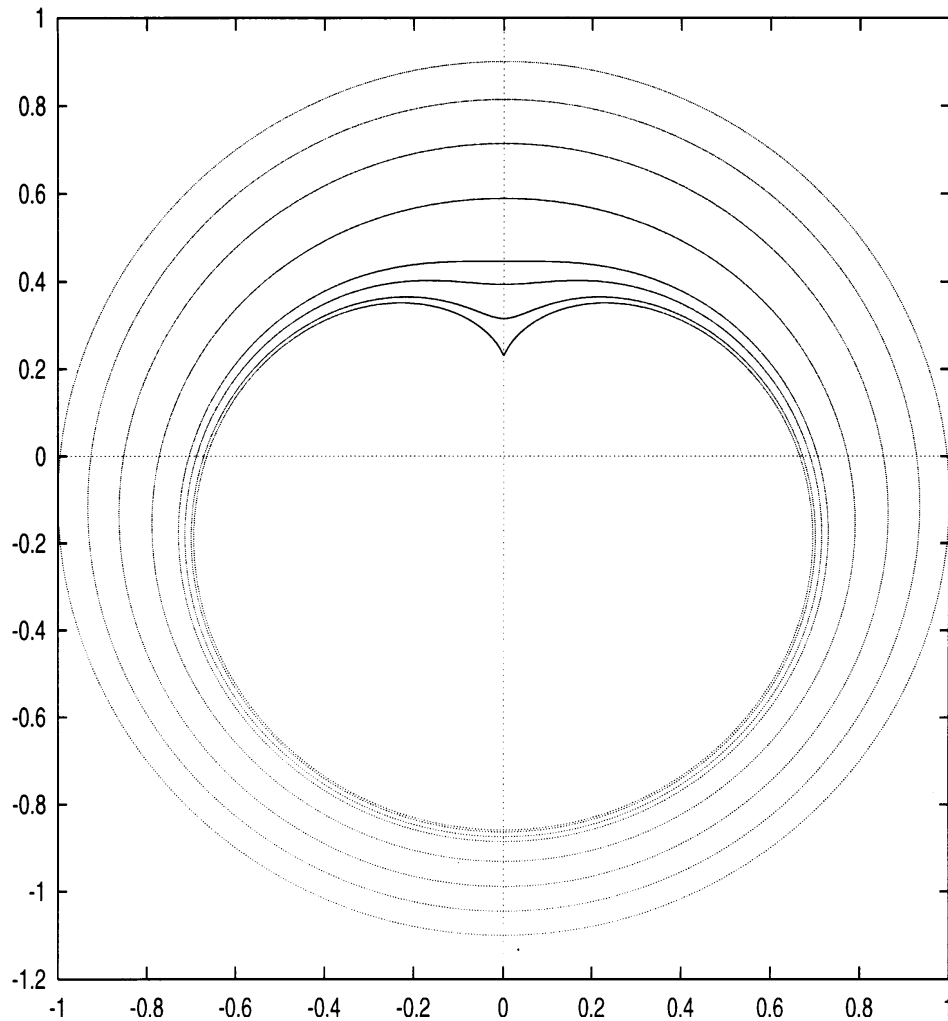


FIGURE 1. Collapse of 10% offset sink for zero surface tension. Plots, from the outer perimeter inwards, are at times $t = 0.0, 5.0, 10.0, 15.0, 19.0, 20.0, 21.0$ and at the formation of the cusp, $t \approx 21.45$.

expanded upon this theory, taking into account multiply-connected domains and barriers, analysing, among others, the situation where air becomes trapped by the advancing fluid and the rigid boundaries.

1.2 Flows with surface tension

For the case of non-zero surface tension, no analytic solution exists for the suction problem. Researchers attempting to tackle this problem analytically have tended to assume, on physical grounds, that surface tension would provide a regularization of the problem, i.e. the presence of surface tension would 'round' the cusp, avoiding the sharpening of the interface, thereby allowing the solution to exist after the break-down time for zero surface tension. Howison *et al.* (1988) looked at both cases of non-zero and the

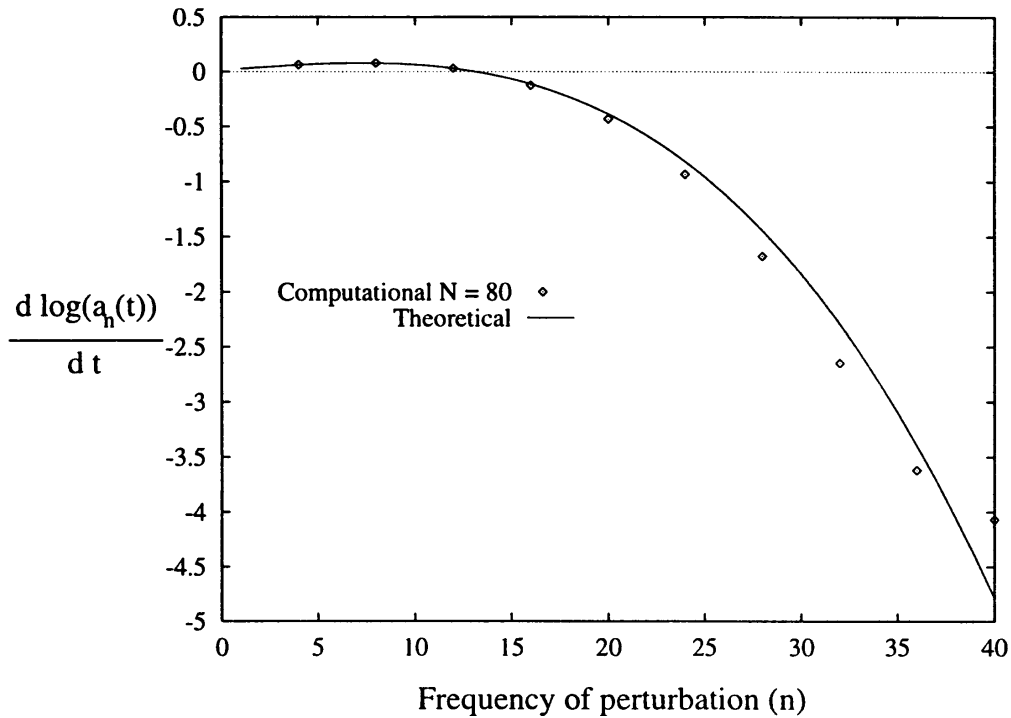


FIGURE 2. Plot of theoretical stability curve and quartic spline results for $\gamma^* = 10^{-3}$.

zero surface tension. For the purposes of their analysis, they set the time of cusp formation to $t = 0$. For the case of small surface tension, they concentrated on the small time behaviour of the interface in the region where a cusp would otherwise have formed.

Hohlov *et al.* (1994) expanded upon the work of Howison *et al.* (1988). They touched briefly upon the idea of a ‘viscosity’ type of regularization, where the free boundary is modelled as a smooth transition layer between the viscous and inviscid regions, but concentrated on two other methods of regularization. The first is the usual introduction of surface tension, giving the ‘Gibbs–Thomson’ condition as they refer to it, the second being a regularization due to kinetic undercooling, which provides the ‘kinetic’ condition where the pressure jump at the interface is proportional to the normal velocity. Their analysis is on such a lengthscale that the ‘crack’ is considered instead as a ‘slit’ of zero thickness, concealing the intricate short wavelength ‘dendritic’ patterns which are frequently observed. This also gets round the ill-posedness of the crack model (it can have singularities, determined by the initial thickness, which cause finite-time blow-up), at the expense of introducing some arbitrariness in the motion of the slit tip.

Both the crack and slit models, however, are incomplete, and a complete analytic solution to the problem remains elusive. Here we apply a boundary integral method to achieve a numerical solution of the problem.

An alternative scenario to the crack/slit model has been investigated by Tanveer (1993), Siegel & Tanveer (1996) and Siegel, Tanveer & Dai (1996). In their analyses, the effect of small surface tension is to produce some ‘daughter singularities’ in a certain complex plane. When these daughter singularities approach the image of the physical boundary, the

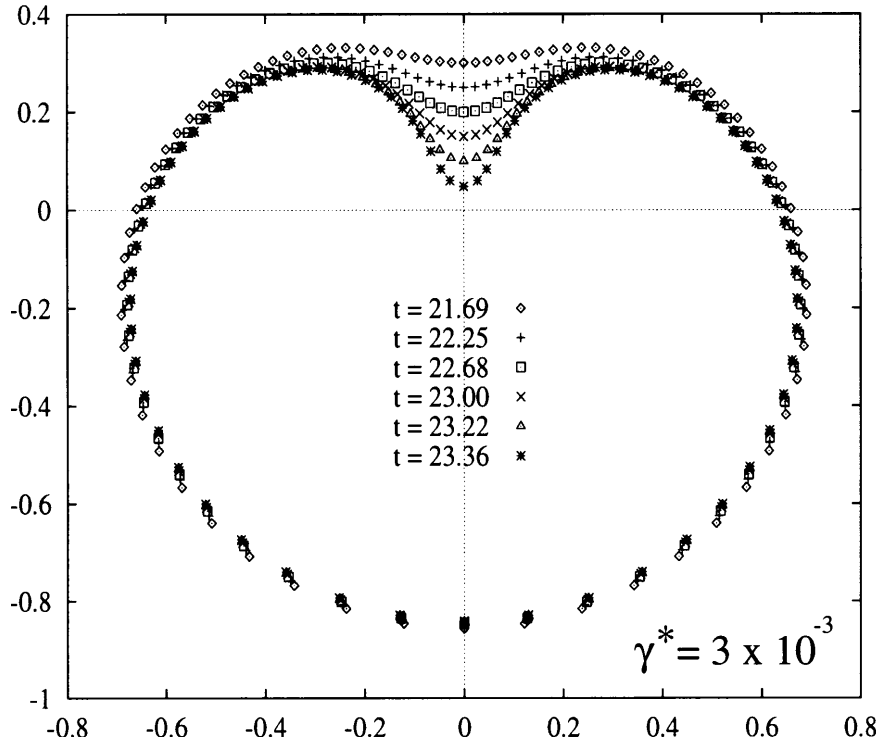


FIGURE 3. Time-lapse picture of the development of the interface at $t = 21.69, 22.25, 22.68, 23.00, 23.22$ and 23.36 with $N = 80$ and $\gamma^* = 3 \times 10^{-3}$.

behaviour changes dramatically from that with zero surface tension. Typically, multi-headed dendritic fingers are formed. No predictions have however been made for the sink flow studied in this paper.

2 Formulation

The basic equations of the sink flow problem are very much the same as those for the quadrupole problem tackled by Kelly & Hinch (1997). The standard theory of flow in a Hele-Shaw cell, as detailed in Lamb (1932), is used. Application of Green's second identity results in

$$\frac{1}{2}p(\mathbf{x}) = -\frac{Q}{2\pi} \ln |\mathbf{x}| + \oint \left(p(\mathbf{x}') \frac{\partial G(\mathbf{x}, \mathbf{x}')}{\partial n'} - G(\mathbf{x}, \mathbf{x}') \frac{\partial p(\mathbf{x}')}{\partial n'} \right) dl', \quad (1)$$

with $G(\mathbf{x}, \mathbf{x}') = 1/2\pi \ln |\mathbf{x} - \mathbf{x}'|$, and \mathbf{x} a point on the viscous-inviscid interface. The first term on the right-hand side of equation (1) corresponds to a point sink at the origin of strength Q ($Q < 0$ gives a point sink, $Q > 0$ a point source).

The velocity of the interfacial point is given by

$$\mathbf{u}(\mathbf{x}) = -\frac{h^2}{12\mu} \nabla p(\mathbf{x}). \quad (2)$$

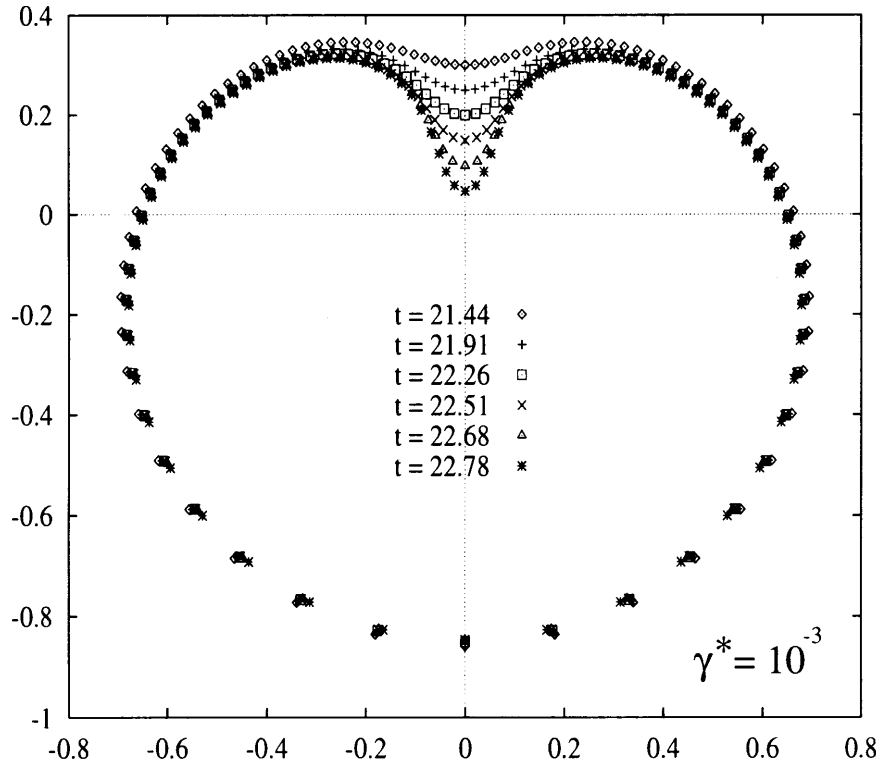


FIGURE 4. Time-lapse picture of the development of the interface at $t = 21.44, 21.91, 22.26, 22.51, 22.68$ and 22.78 with $N = 80$ and $\gamma^* = 10^{-3}$.

At the interface we have a pressure jump due to surface tension, such that

$$p(\mathbf{x}) = \gamma\kappa(\mathbf{x}), \quad (3)$$

where γ is the surface tension coefficient (assumed constant), and $\kappa(\mathbf{x})$ is the local curvature. We ignore the Park & Homsy (1984) factor here.

As this is effectively a two-dimensional problem, we choose to rescale all our lengths by the initial radius of the fluid blob, D . This allows us to rewrite equation (1), highlighting the two competing flow driving forces, as,

$$p = O(Q) + O\left(\frac{\gamma}{D}\right). \quad (4)$$

This gives us our dimensionless surface tension coefficient as $\gamma/|Q|D$, which we denote by γ^* . We non-dimensionalize the pressure with Q , lengths by D , velocities with $h^2|Q|\mu D$, and therefore the time by $\mu D^2/h^2|Q|$.

3 Richardson's solution for zero surface tension

As mentioned in the introduction, Richardson (1972) in a worked example provides the exact solution for the off-centre sink with zero surface tension. The shrinkage of an initially circular blob with 10% off-set sink is depicted in Figure 1 to the time of cusp formation

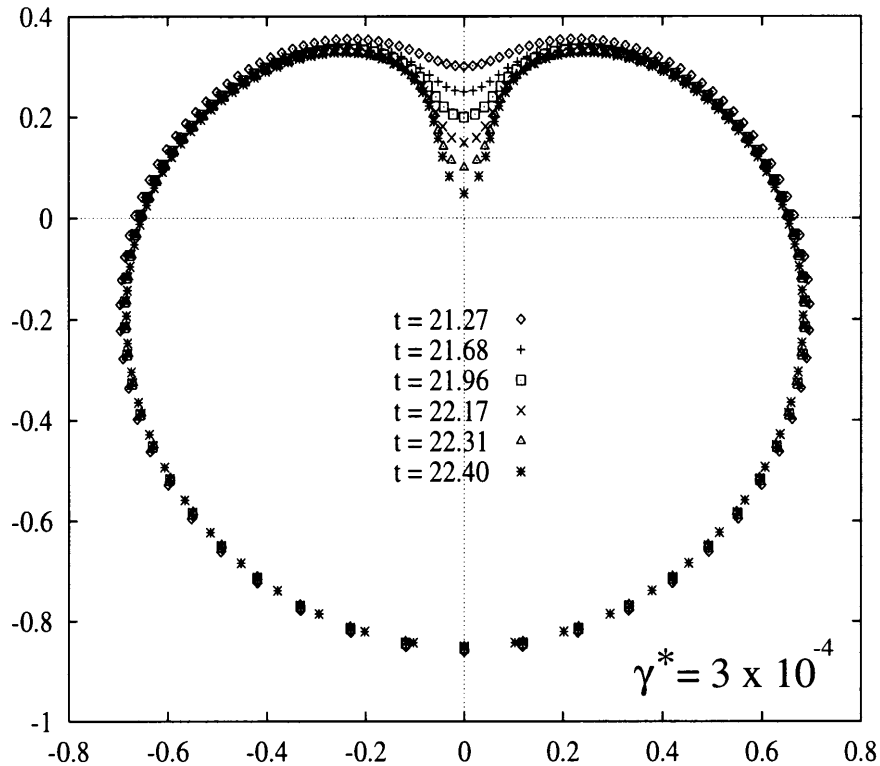


FIGURE 5. Time-lapse picture of the development of the interface at $t = 21.27, 21.68, 21.96, 22.17, 22.31$ and 22.40 with $N = 100$ and $\gamma^* = 3 \times 10^{-4}$.

at $t \approx 21.45$, with snapshots at regular time intervals until close approach to the cusp. The singularity in the curvature of the interface is of the form of a $3/2$ power-law cusp.

4 Numerical method

The basic numerical techniques employed in this problem are to a great extent very similar to those employed in Kelly & Hinch (1995). The N points on the viscous–inviscid interface are interpolated by a quartic spline, with the x and y coordinates interpolated independently, in each case the spline parameter τ having unit range between neighbouring points, e.g. $\mathbf{x}_1 \equiv \mathbf{x}(\tau = 1)$, $\mathbf{x}_2 \equiv \mathbf{x}(\tau = 2)$, etc.

The curvature κ at a point \mathbf{x} is then given by

$$\kappa = \frac{x_\tau y_{\tau\tau} - y_\tau x_{\tau\tau}}{(x_\tau^2 + y_\tau^2)^{3/2}}, \quad (5)$$

and the outward normal \mathbf{n} as

$$\mathbf{n} = \frac{(y_\tau, -x_\tau)}{\sqrt{x_\tau^2 + y_\tau^2}}. \quad (6)$$

Due to an eigensolution of (1) with zero eigenvalue corresponding to $p = \text{const.}$ producing no flow ($\partial p / \partial n = 0$), the matrix of the discretized form was purged, by adding a product of this eigenvector and its adjoint which changes the eigenvalue from zero. The

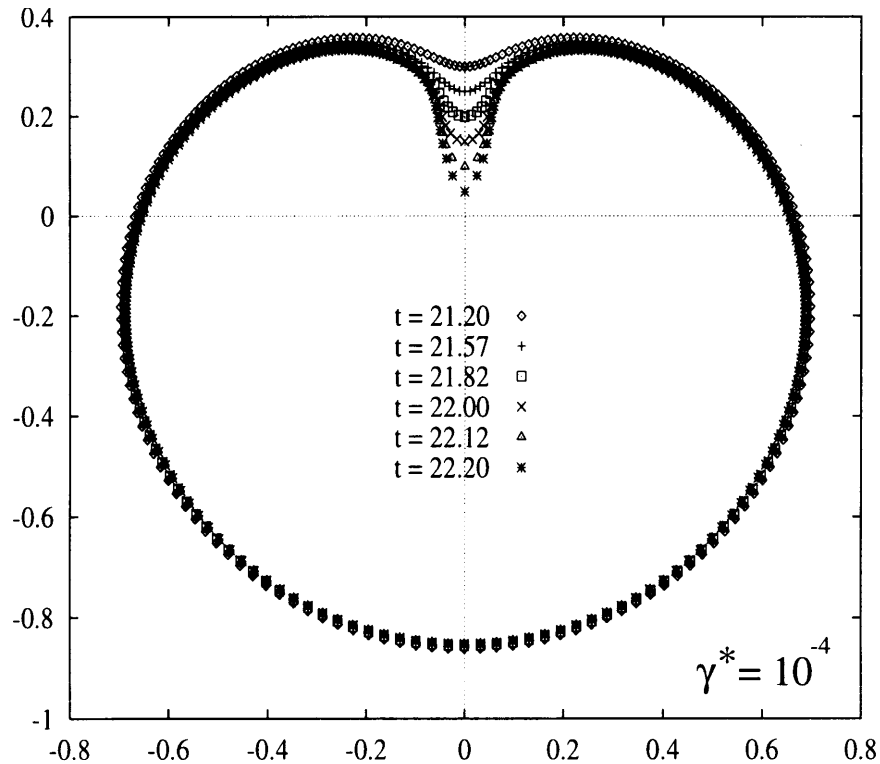


FIGURE 6. Time-lapse picture of the development of the interface at $t = 21.20, 21.57, 21.82, 22.00, 22.12$ and 22.20 with $N = 200$ and $\gamma^* = 10^{-4}$.

motion due to the presence of the sink was imposed after elimination of spurious area changes. Tests of the accuracy of the methods employed are detailed in Kelly & Hinch (1995). Savings in computations were made by taking advantage of the symmetry of the fluid drop about the y -axis.

Tangential redistribution of the boundary nodes was also employed. Here it was used to pack actively certain areas of the interface where greater detail was needed, at the expense of sections where little change occurs. As it was assumed that the solution for small surface tension would be similar to the case of zero surface tension, observation of Figure 1 showed that the greater part of the motion of the interface occurs in a small wedge about the positive y -axis, and thus the tangential motion of the nodes was augmented to ensure a greater density in this region. Later results revealed the development of a thin, rapidly moving, inviscid finger with high tip curvature in the cusp region which necessitated a weighting in favour of regions of high curvature in the redistribution algorithm.

5 Stability analysis

The sink flow with zero surface tension is highly unstable to small perturbations, to the extent of being an ill-posed problem. As a further and demanding test of the numerical method, the stability of the concentric sink flow was examined with small non-zero surface tension. The growth of a small perturbation of the form $a_n \cos(n\theta)$, $n \in \mathbb{N}$, $-\pi \leq \theta \leq \pi$, on

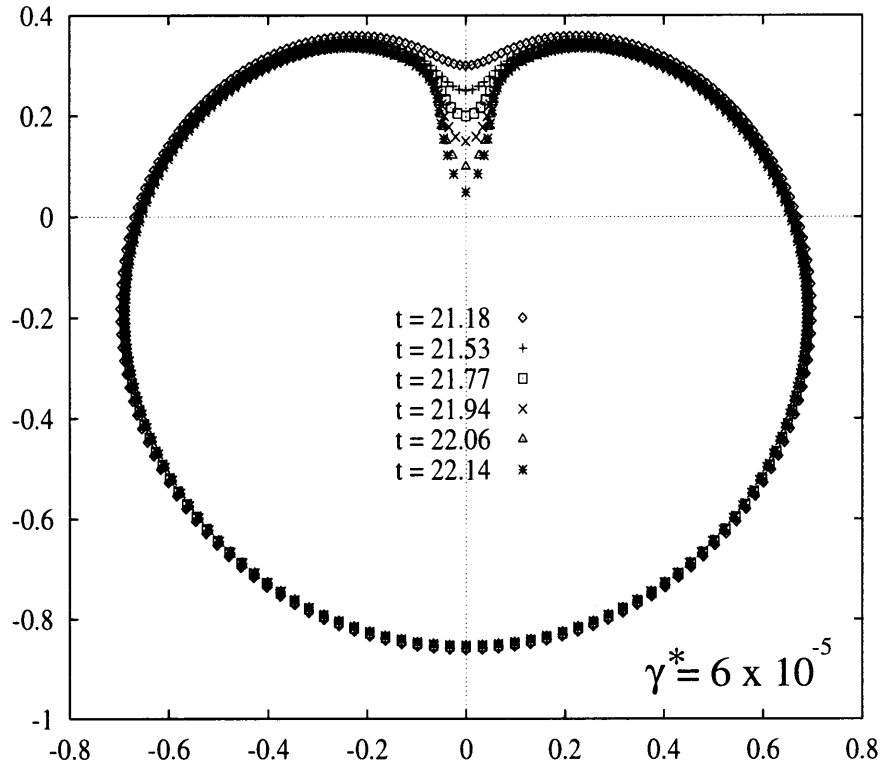


FIGURE 7. Time-lapse picture of the development of the interface at $t = 21.18, 21.53, 21.77, 21.94, 22.06$ and 22.14 with $N = 200$ and $\gamma^* = 6 \times 10^{-5}$.

a circular drop of radius $R_0(t)$, centred on the sink, was studied. Linear stability analysis gives

$$\frac{d \ln(a_n(t))}{dt} = \frac{1}{12} \left\{ \frac{(n+1)}{2\pi R_0^2} - \frac{\gamma^*(n^2-1)n}{R_0^3} \right\}, \quad (7)$$

which we will refer to as the perturbation growth equation.

As can be seen in equation (7), there are two competing effects in the development of the disturbance. The first term in brackets on the right-hand side of equation (7) represents the destabilizing effect of the sink flow. The second term represents the stabilizing effect of surface tension, smoothing out noise.

The numerical code was then tested against this result. A sinusoidal perturbation of $O(10^{-6})$ was placed upon a circular drop of unit radius, with $\gamma^* = 10^{-3}$, and the growth of the disturbance was analysed at $t = 1$. The results of this test is displayed in Figure 2, where we plot $\ln(a_n(1)/a_n(0))$.

Note how the matching is excellent for the lower modes, but loses accuracy as n is increased. This is due to the interpolating spline being less and less able to give accurately the curvature of the higher order perturbations.

Similar tests were also carried out to study the damping effect of surface tension on Gaussian random noise imposed initially. Due to centre of gravity and area perturbations resulting from the imposition of noise, all analysis was carried out via the local curvatures,

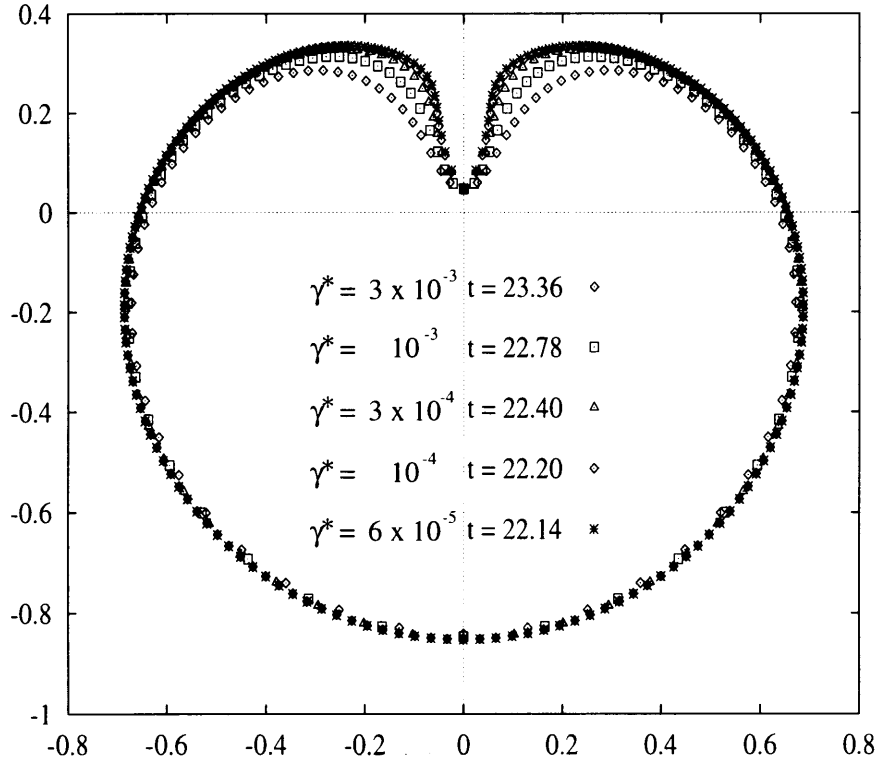


FIGURE 8. Comparison of finger widths for a sequence of surface tension strengths. $y_t = 0.05$ in each case. The time for the tip to reach this point is also recorded.

rather than the actual position of the boundary nodes. The noise was found to behave as predicted by the perturbation growth equation for a range of values of γ^* .

Requiring that at least the top half of the $N/2$ possible numerical wavenumbers are physically stable leads to a restriction on the number of nodes required:

$$N > 1.6\gamma^{*-1/2}. \quad (8)$$

6 Results

The initial conditions for each experimental run were similar. The interface was set up with the nodes evenly distributed on a circle of radius 1, with its centre at the point $(0.0, -0.1)$. The sink was placed at the origin, i.e. 10% offset from the centre of the initial circle.

6.1 Evolution of a finger

The shape of the interface as it approaches the sink is illustrated for a range of values of γ^* in Figures 3–7. The particular snapshots of the development of the drop are for times corresponding to $y_t = 0.3$ down to $y_t = 0.05$, at intervals of 0.05, where y_t denotes the height of the finger tip above the sink. Of note in each of these pictures is the relative immobility of much of the interface as the finger forms, with most of the action taking place

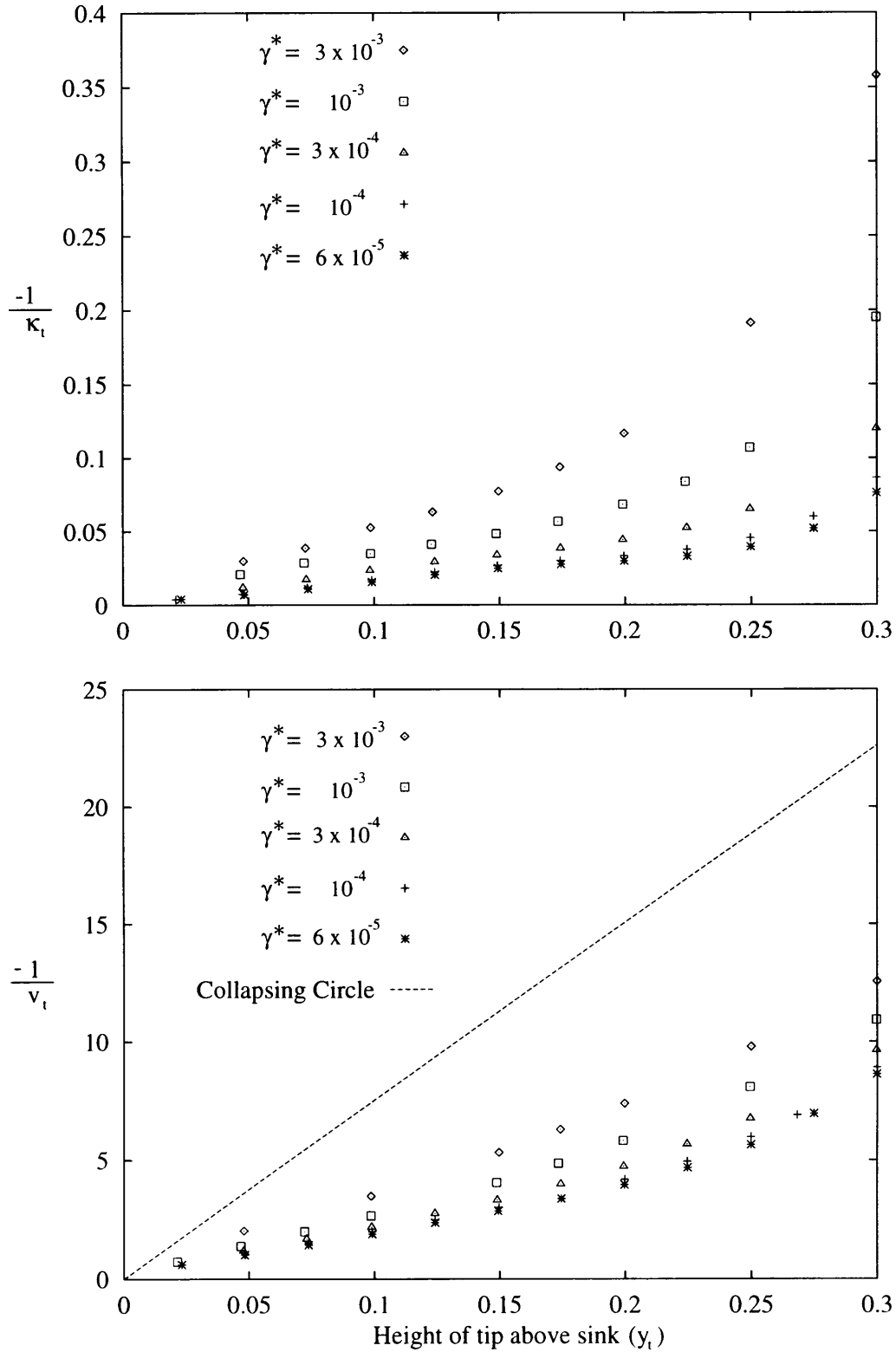


FIGURE 9. Plots of the decrease in $-1/\kappa_t$ and $-1/v_t$ as the sink is approached.

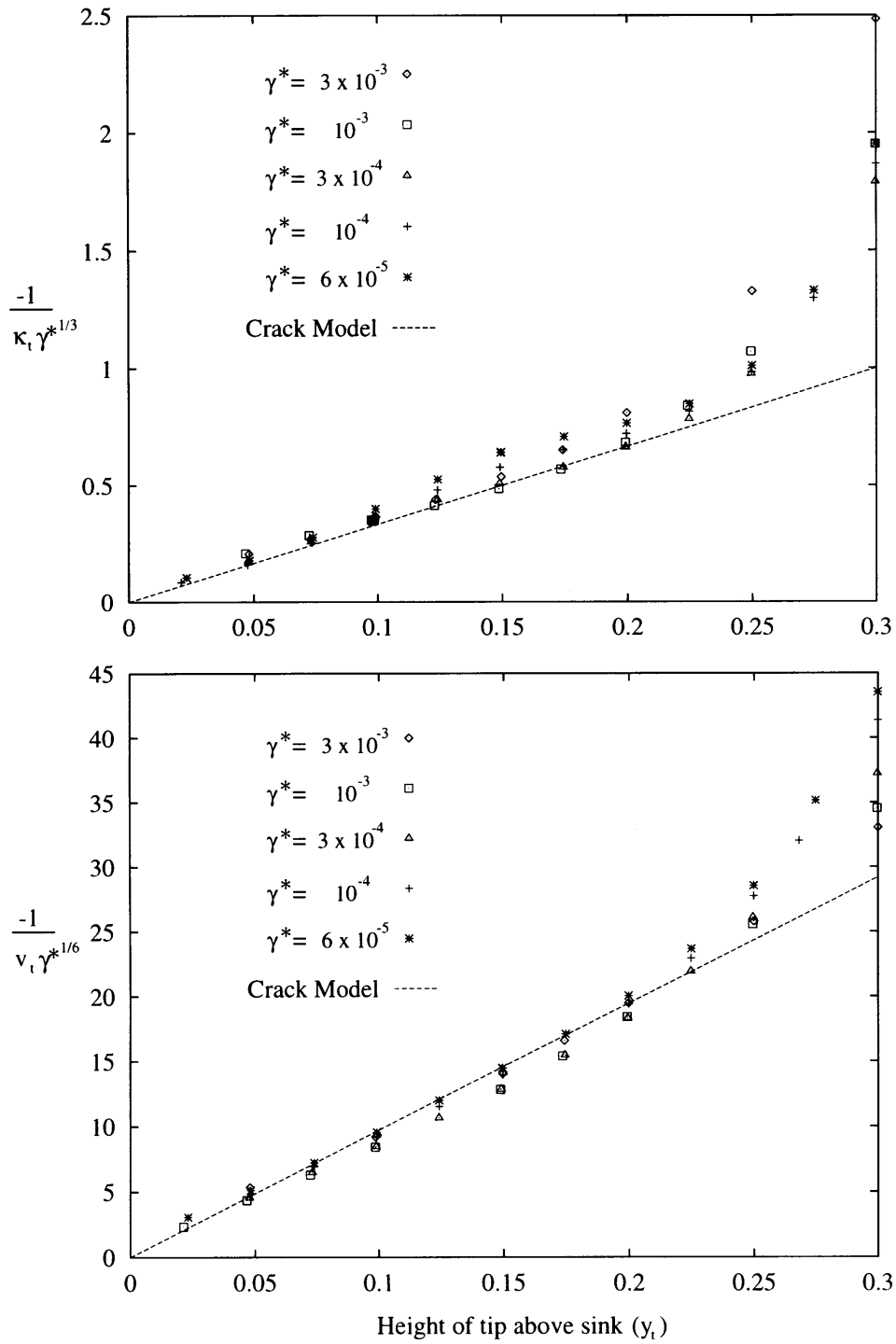


FIGURE 10. (a) Collapse of curvature plots, showing 1/3 power-law dependence of $-1/\kappa_t$ on γ^* ; (b) collapse of velocity plots, showing 1/6 power-law dependence of $-1/v_t$ on γ^* . The dotted line is the prediction from the crack model of §6.6.

in a tight wedge about the positive y -axis. All the simulations with surface tension continue beyond $t = 21.45$ when a cusp forms with zero surface tension at $y_t = 0.232$.

6.2 Comparison of finger widths

Figure 8 illustrates the variation of the width of the inviscid finger with surface tension. The range is as previously covered in the time-lapse figures. In each case $y_t = 0.05$. Note how the finger gradually narrows as γ^* decreases. Also of note is that the time for the tip to reach the height of observation diminishes with the surface tension.

6.3 Curvature and velocity scalings with the surface tension

The behaviour of the local curvature at the tip, κ_t , and the velocity of the tip, v_t , as the sink is approached is depicted in Figure 9 for the range of surface tension values considered. In both cases, since the quantities go to negative infinity at the sink, their negative inverses are plotted as functions of the distance of the tip from the sink y_t . Note that the fingers move towards the sink faster than the circle would have if it had zero offset, as given by the dotted line. The fingers move faster because almost all the constant flow into the sink comes from the small sector of the finger, and thus the velocities of the fingers are inversely proportional to their width.

Given the behaviour illustrated in Fig. 9, a power-law dependence on the surface tension was sought, i.e. tests were made to find an m such that at each y_t

$$-\frac{1}{\kappa_t} \propto \gamma^{*\frac{1}{m}}. \quad (9)$$

The best fit for the data was found to be for $m = 3$, as illustrated in Figure 10. The fit is good over the range displayed, which as Figure 3 to 7 show is the limit of the existence of the finger. The stray points at $y_t = 0.25$ and 0.3 for $\gamma^* = 3 \times 10^{-3}$ are due to the interface only having just begun to show signs of finger development, as can be seen in Figure 3.

Similarly, a power-law dependence on the surface tension was sought for $-1/v_t$. Excellent matching was achieved for $m = 6$ over the range of interest, as can also be seen from Figure 10.

6.4 Self-similar shape of the fingers

Now we have seen in Figure 9 that for a given value of the surface tension γ^* the radius of curvature of the tip $-1/\kappa_t$ is proportional to the distance of the tip from the sink y_t . In Figure 11, for two different values of the surface tensions, we superpose fingers at different times by scaling with y_t , i.e. plotting x and y each divided by $y_t(t)$. We see that the rescaled curvature at the tip remains constant, as given earlier in Figure 9. We also see that as the finger grows in time it asymptotes to a fixed shape (in these rescaled coordinates).

Now Figure 10 showed additionally that the curvature of the tip at any y_t was proportional to $\gamma^{*-1/3}$. We have therefore superposed fingers at different γ^* for $y_t = 0.1$ by rescaling the width of the fingers with $\gamma^{*-1/6}$, i.e. plotting y/y_t against $x/y_t \gamma^{*1/6}$, as may be seen in Figure 12. We see that the shapes agree not only at the tip, but also as far as the

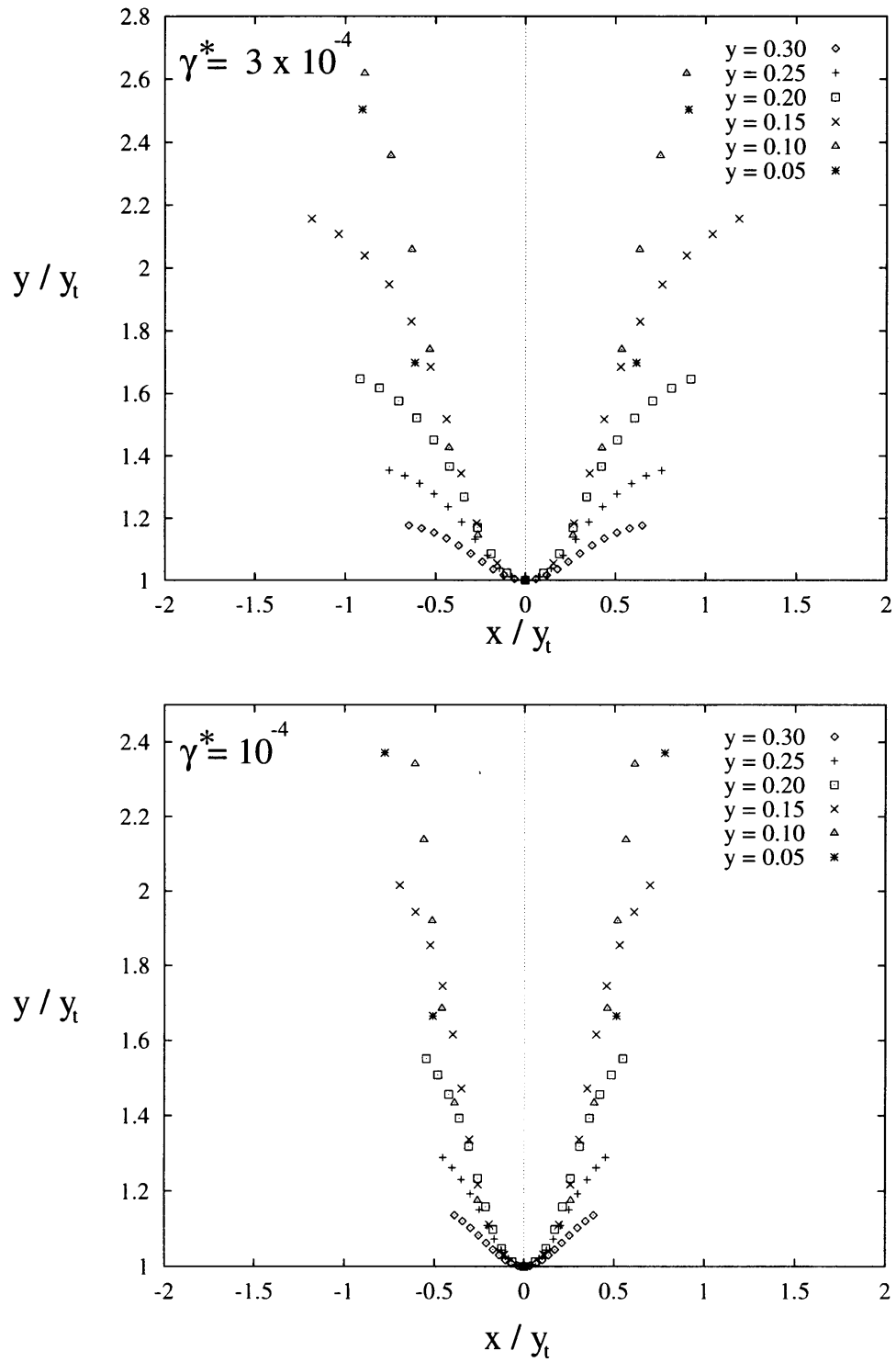


FIGURE 11. Superposition of fingers scaled by $y_t = 0.3, 0.25, 0.2, 0.15, 0.1$ and 0.05 , with $\gamma^* = 3 \times 10^{-4}$ and 10^{-4} .

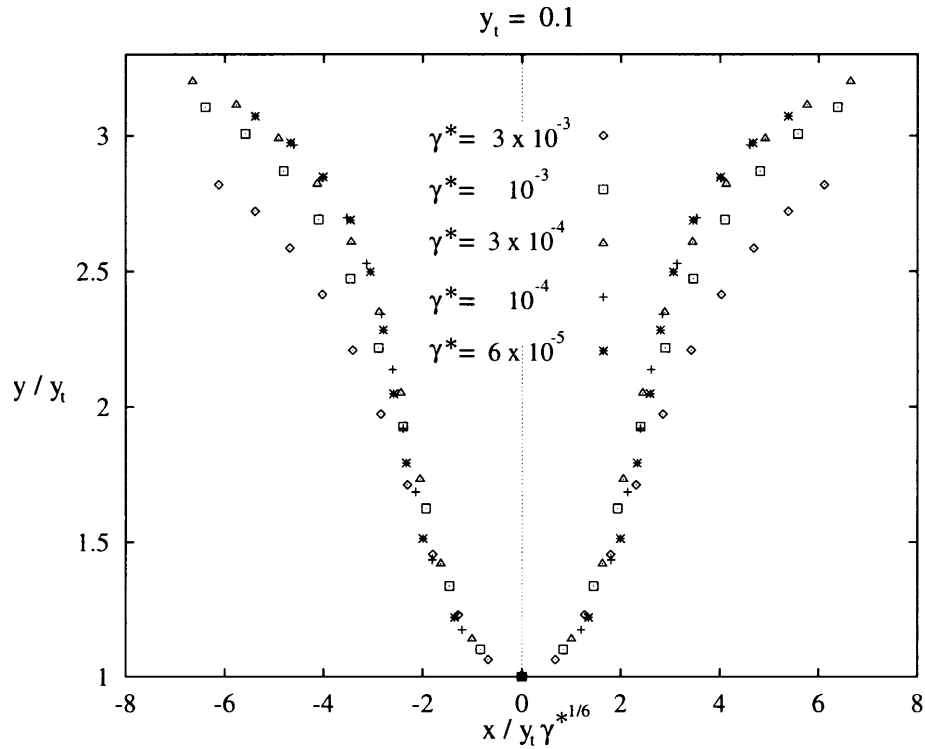


FIGURE 12. Superposition of fingers for a range of values of γ^* with $y_t = 0.1$, scaled by y_t in the y -coordinate and $y_t \gamma^{*1/6}$ in the x -coordinate.

fingers are formed. The fingers thus seem to adopt a universal self-similar form, at least for the 10% offset sink.

6.5 Effect of offset shift

The effect of a shift in the position of the sink was also observed. A 20% offset sink, with the blob initially centred at $(0.0, -0.2)$ and surface tension $\gamma^* = 3 \times 10^{-4}$ was chosen. Figures 13 and 14 illustrate the effect of this shift in comparison with the previous results for $\gamma^* = 3 \times 10^{-4}$ with the 10% offset. In Figure 13 we see that although the viscous finger forms much earlier for the 20% offset case, the dimensions of the finger itself are unaffected. This is borne out in the succeeding comparisons of the curvature and velocity of the tip in Figure 14. Thus once the fingers form their shape and behaviour does not depend on the particular value of the offset.

6.6 Relation between curvature and velocity of the tip

In an attempt to explain the scalings of κ_t and v_t , we consider modelling the inviscid finger as a thin crack along the positive x -axis (for convenience of this subsection), with the tip very near to the origin and the sink at $(-a, 0)$. Under the transformation $z = \zeta^2$ with

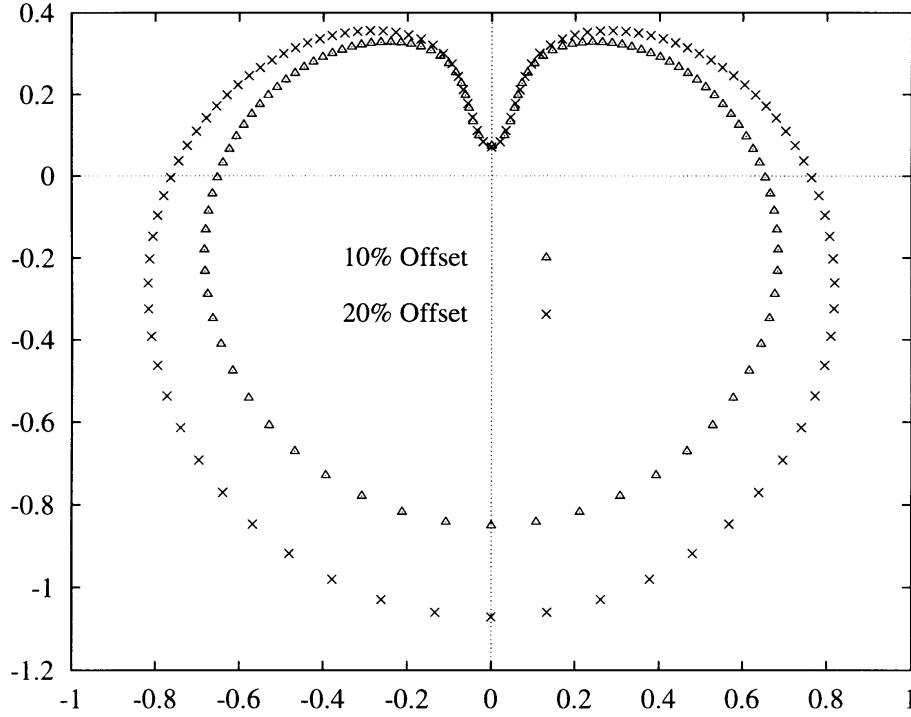


FIGURE 13. Comparison of finger widths for 10% and 20% offset sinks, with $\gamma^* = 3 \times 10^{-4}$. 10% offset case is at $t = 22.3575$. 20% offset case is at $t = 15.395$.

$x = x + iy$ and $\zeta = \xi + i\eta$, the crack becomes stretched out near to the ξ -axis with a sink at $(0, \sqrt{a})$. If we assume that the crack is approximately a $p = \text{const.}$ surface near to the ξ -axis, then we need an image source at $(0, -\sqrt{a})$. The expression for the pressure is then

$$p = \Re \left\{ \frac{1}{2\pi} \ln \left(\frac{\zeta - i\sqrt{a}}{\zeta + i\sqrt{a}} \right) \right\}. \quad (10)$$

Near to the tip of the crack, $\zeta \ll \sqrt{a}$

$$p \sim \Re \left\{ \frac{i}{\pi} \frac{\zeta}{\sqrt{a}} \right\} = \Re \left\{ \frac{i z^{1/2}}{\pi \sqrt{a}} \right\} = -\frac{1}{\pi} \sqrt{\frac{r}{a}} \sin \frac{\theta}{2} \quad (11)$$

in polar coordinates. The local velocity near the tip is

$$v|_{\theta=\pi} = -\frac{1}{12} \frac{\partial p}{\partial r} \Big|_{\theta=\pi} = \frac{1}{24\pi \sqrt{ar}}. \quad (12)$$

Now we have assumed that the crack is a $p = \text{const.}$ surface, i.e. a $\eta = \text{const.}$ surface. Then using $x + iy = \xi^2 - \eta^2 + 2i\xi\eta$, so $\xi = y/2\eta$, we find this surface is

$$x(y) = -\eta^2 + \frac{y^2}{4\eta^2}, \quad (13)$$

which has a curvature at $y = 0$ of

$$x_{yy} = \frac{1}{2\eta^2}. \quad (14)$$

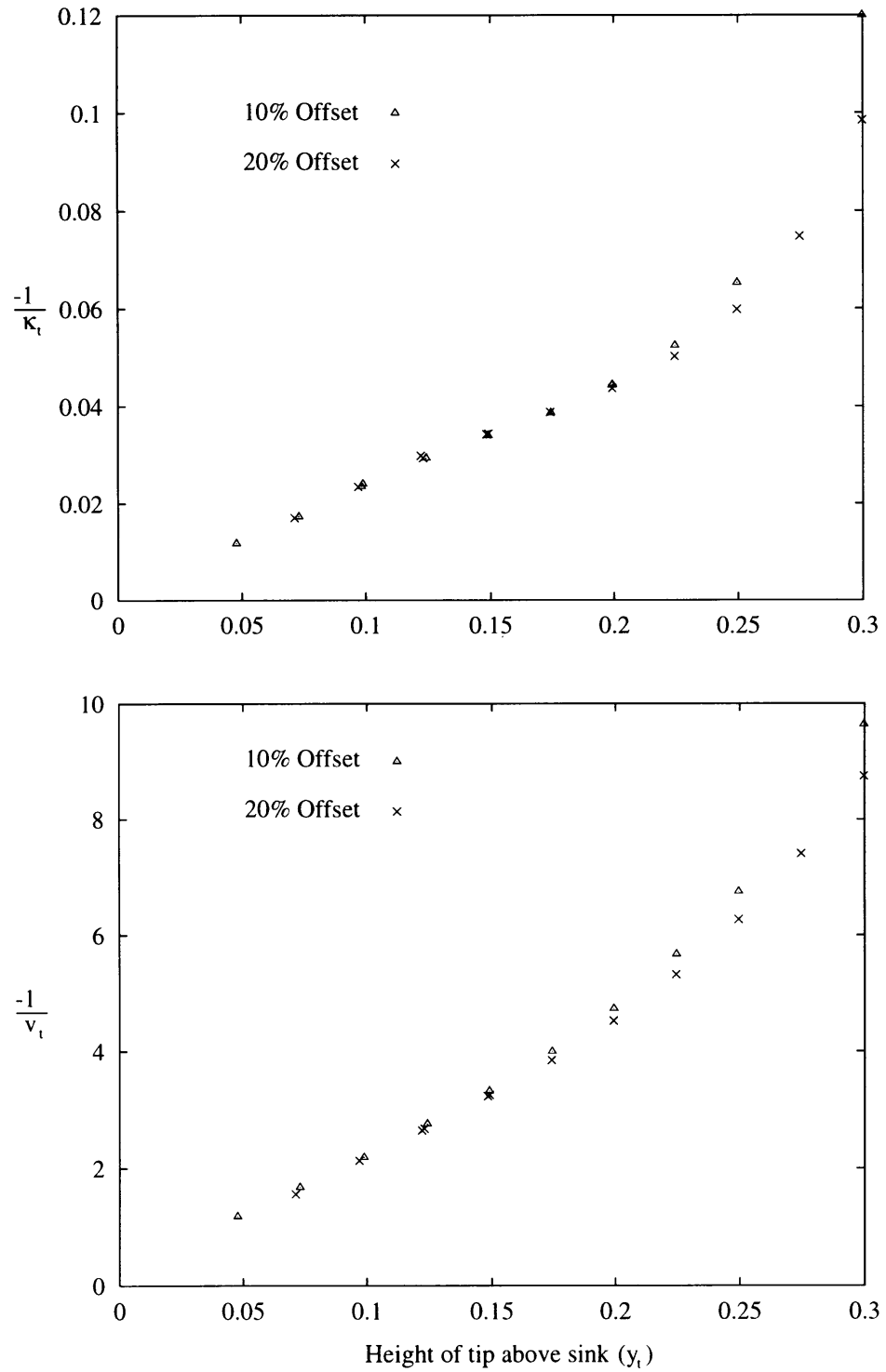


FIGURE 14. Comparison of the decrease in $-1/\kappa_t$ and $-1/v_t$ as the sink is approached for 10% and 20% offset sinks, with $\gamma^* = 3 \times 10^{-4}$.

Now in our numerical simulations we find the curvature of the tip

$$\kappa_t = -\frac{k}{a}\gamma^{*-1/3}, \quad (15)$$

with $k \approx 0.3$. This gives at $y = 0$

$$r = -x = \eta^2 = \frac{1}{2\kappa} = \frac{a}{2k}\gamma^{*1/3}. \quad (16)$$

Hence, the above model predicts that the velocity of the tip is

$$v_t = \frac{\gamma^{*1/6}}{a} \frac{\sqrt{2k}}{24\pi}. \quad (17)$$

The expressions for κ_t and v_t for $k = 0.3$ are plotted in Figure 10. We see that Laplace's equation successfully links the scalings of κ_t and v_t .

It should be noted that the model is based on the assumption that the interface has $p = \text{const}$. The precise value at the tip is $\gamma^{*1/6}/\pi\sqrt{2k}$, which is very much larger than the capillary pressure $\gamma^*\kappa = k\gamma^{*2/3}/a$ while $a \gg \gamma^{*1/2}\pi k^{3/2}\sqrt{2}$.

7 Conclusions

The results of our simulations confirm what has been the generally accepted hypothesis as to the behaviour of the fluid once surface tension forces are included. The solution exists well beyond the time of cusp formation for the case of zero surface tension, forming a narrow, rounded finger where before a $3/2$ power-law cusp was evident, thus demonstrating the singular perturbation nature of the problem. Certain interesting features of this finger have been revealed. Its width diminishes with the surface tension of the fluid, with the curvature of the tip region having a $1/3$ power-law dependence on γ^* . The speed at which the tip approaches the sink also depends on the surface tension, in this case in the form of a $1/6$ power-law. This contradicts Howison *et al.* (1988), who suggest a $2/3$ power-law dependence on γ^* for the tip curvature and a $1/3$ power-law for the velocity. At this time we are unable to offer any explanation for the scalings found in our simulations. We note, however, that the model of Howison *et al.* assumes a steady state finger which is not possible in the continually converging geometry of the sink flow.

The simulations have further shown that the fingers adopt a self-similar shape as they approach the sink, a shape which does not depend on the value of the initial offset of the sink, a shape whose width scales with $\gamma^{*1/6}$.

The shape of the self-similar finger is simple and not the dendritic form caused by daughter singularities as in Siegel, Tanveer & Dai (1996). We suggest for the sink flow that the daughter singularities must remain further from the image of the physical boundary than the zero of the original zero-surface-tension map. One interesting feature of the analysis of Tanveer (1993) is the existence of a $\gamma^{*1/6}$ scaling. We are, however, unable to identify the physical balance responsible for this scaling which might then be applied to the sink problem of this paper.

The computations were supported [in part] by the SERC ‘Computational Science Initiative’ Grant GR/H57585.

References

- BATCHELOR, G. K. (1967) *An Introduction to Fluid Dynamics*. Cambridge University Press.
- DiBENEDETTO, E. & FRIEDMAN, A. (1984) The ill-posed Hele-Shaw model and the Stefan problem for supercooled water. *Trans. Am. Math. Soc.* **282**, 183–204.
- HOHLOV, Y. E., HOWISON, S. D., HUNTINGFORD, C., OCKENDON, J. R. & LACEY, A. A. (1994) A model for non-smooth free boundaries in Hele-Shaw flows. *Quart. J. Mech. Appl. Math.* **47** (1), 107–128.
- HOWISON, S. D., OCKENDON, J. R. & LACEY, A. A. (1985) Singularity development in moving boundary problems. *Quart. J. Mech. Appl. Math.* **38**, 343–360.
- HOWISON, S. D., LACEY, A. A. & OCKENDON, J. R. (1988) Hele-Shaw free-boundary problems with suction. *Quart. J. Mech. Appl. Math.* **41**, 183–193.
- KELLY, E. D. & HINCH, E. J. (1997) Numerical solutions of a multipole problem in the Hele-Shaw cell. *Euro. J. Applied Math* (to appear).
- POLUBARINOVA-KOCHINA, P. YA. (1945) On the motion of the oil contour. *Doklad Akad. Nauk. SSSR* **47** (4), 254–257.
- PARK, C.-W. & HOMS, G. M. (1984) Two-phase displacement in Hele-Shaw cells: theory. *J. Fluid Mech.* **139**, 291–308.
- RICHARDSON, S. (1972) Hele-Shaw flows with a free boundary produced by the injection of fluid into a narrow channel. *J. Fluid Mech.* **56**, 609–618.
- RICHARDSON, S. (1994) Hele-Shaw flows with time-dependent free boundaries in which the fluid occupies a multiply-connected region. *Euro. J. Applied Math.* **5**, 97–122.
- SAFFMAN, P. G. & TAYLOR, G. I. (1958) The penetration of a fluid into porous medium or Hele-Shaw cell containing a more viscous liquid. *Proc. R. Soc. A* **245**, 312–329.
- SIEGEL, M. & TANVEER, S. (1996) Singular perturbation of smoothly Hele-Shaw solutions. *Phys. Rev. Lett.* **76**, 419–422.
- SIEGEL, M., TANVEER, S. & DAI, W.-S. (1996) Singular perturbation of smoothly evolving zero surface tension solutions in a Hele-Shaw cell – comparison between asymptotics and numerics. *J. Fluid Mech.* **323**, 201–236.
- TANVEER, S. (1993) Evolution of Hele-Shaw interface for small surface tension. *Phil. Trans. R. Soc. Lond. A* **343**, 155–204.